



In situ synthesis of carbon-doped TiO₂ single-crystal nanorods with a remarkably photocatalytic efficiency



Jian Shao^a, Weichen Sheng^{a,*}, Mingsong Wang^a, Songjun Li^a, Juanrong Chen^b, Ying Zhang^a, Shunsheng Cao^{a,*}

^a Institute of Polymer Materials, School of Materials Science and Engineering, Jiangsu University, Zhenjiang 212013, China

^b School of Environment and Safety Engineering, Jiangsu University, Zhenjiang 212013, China

ARTICLE INFO

Article history:

Received 20 January 2017

Received in revised form 22 February 2017

Accepted 1 March 2017

Available online 2 March 2017

Keywords:

TiO₂ single crystal

Carbon-doped TiO₂ nanorods

In situ synthesis

Visible-light photocatalytic activity

ABSTRACT

Incorporating dopants into the TiO₂ single crystals lattice is a big challenge because single crystal has a high crystallinity and the nucleation and growth of TiO₂ single crystals is readily subjected to the interference of the dose of dopant precursors. Here, we propose an *in situ* synthetic strategy for the construct of carbon-doped TiO₂ single crystal nanorods using CPS/TiO₂ as the precursors of TiO₂ nanorods and carbon source *via* a facile hydrothermal route. This technique involves the preparation of cationic polystyrene spheres (CPS), sequential deposition of TiO₂ precursor, hydrothermal reaction, and the pyrolysis of CPS in a N₂ atmosphere at 450 °C. The morphology and structure of as-prepared C-TiO₂ single crystal nanorods were characterized by TEM, SEM, STEM Mapping, XRD, UV-vis spectroscopy, and XPS. All results confirm the carbon doping in the as-prepared TiO₂ single crystal nanorods. As a result of unique microstructure, the resulting TiO₂ exhibits remarkably visible-light photocatalytic efficiency for the degradation of organic pollutants including methylene blue (MB), Rhodamine B (RhB) and *p*-nitrophenol (PNP). Therefore, the current study provides a new insight for incorporating dopants into the TiO₂ single crystals lattice.

© 2017 Elsevier B.V. All rights reserved.

1. Introduction

Titanium dioxide (TiO₂) has received special interest for its fascinating properties and many promising applications in environmental, catalysis and energy areas [1–3], however, undesired recombination of photo-generated carries can readily occur in the bulk and on the surface of TiO₂, resulting in considerable energy consumption and low degradation efficiency of organic contaminants [3–5]. Undoubtedly, how to efficiently enhance the separation and transfer of photo-generated electron/hole is vital for photocatalytic water treatment.

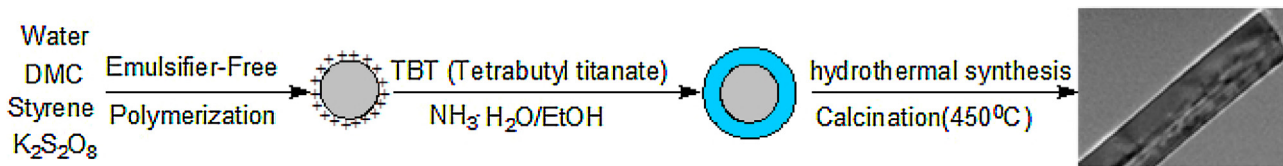
Persistent efforts have been paid to tackle these challenges by doping with metal and/or nonmetal elements, or by incorporating additional components in TiO₂ structure [1,4]. Metal-doped TiO₂ is easily subjected to photo-corrosion, poor thermal stability, and serves as recombination centers due to the dopants' localized d-states deep in the band gap of TiO₂ [4,6], by contrast, non-metal (C, N, B, etc.) doping exhibits a higher efficiency than metal deco-

rating in shifting the ultra-violet of titania to visible-light driven photocatalysis [4,7]. Among them, carbon doping holds potential advantages over other types of nonmetal doping due to its unique properties including large electron-storage capacity, wide range of visible light absorption, and high absorption of organic pollutants, enhancing electronic conductivity and facilitating charge transfer from the bulk of the TiO₂ to the surface region where the desired oxidation reaction occur [4,8]. Many attempts to design carbon-doped TiO₂ have been explored to enhance the photocatalytic behaviors. Liu et al. prepared carbon-doped mesoporous anatase TiO₂ and obtained a significantly enhanced visible-light photocatalytic activity for the degradation of methyl orange [9]. Recently, we explored a facile method for the construction of carbon-doped TiO₂ hollow spheres and demonstrated that the C/TiO₂ photocatalyst exhibited an enhanced visible-light photocatalytic activity for the degradation of Rhodamine B [4]. However, many methods to incorporate carbon element to TiO₂ lattice have limitations because the addition of external carbon precursors (e.g., L-lysine [10], chitosan [11], etc.) is required. Especially, most of the previous works have used polycrystalline TiO₂ as matrix [4,12–14] leading to a lower photocatalytic efficiency.

Compared with those of TiO₂ nanostructures in the form of nanoparticles, polycrystalline nanowires and nanotubes, single

* Corresponding authors.

E-mail addresses: wilson.sheng@gmail.com (W. Sheng), sscaochem@hotmail.com, sscao@ujs.edu.cn (S. Cao).



Scheme 1. The illustration of C-TiO₂ single crystal nanorods.

crystal TiO₂ has attracted increasing interest because of its continuous and ordered interior crystal structure that can hold a much higher electronic conductivity and lower electron transfer resistance, providing direct pathways for efficient separation and transfer of photo-generated carriers and organics decomposition [15–17]. For example, Xiong et al. [18] prepared rutile TiO₂ single crystal nanorods with excellent photocatalytic activity for the degradation of phenol and methylene green. Snaith et al. [19] prepared mesoporous TiO₂ single crystals with enhanced mobility and optoelectronic device performance *via* a seeded template bottom-up synthesis method. Wang et al. [20] reported a facile method to prepare single crystal TiO₂ nanorods and found that as-synthesized TiO₂ exhibited an enhanced photocatalytic activity for the degradation of organic pollutants. Up to now, the synthesis of TiO₂ single crystals has been reported, but mainly focused on the fabrication and construction of single crystals TiO₂ with different facets (e.g., 101, 001 and 100) [21–23] and mesoporous structures, [19,24,25] suggesting that TiO₂ single crystals for photocatalytic water treatment is limited solar energy utilization capacity [4]. Although polycrystalline TiO₂ can be shifted to visible-light driven photocatalysis by doping with metal/nonmetal elements, especially carbon, it is hard to incorporate dopants into the TiO₂ single crystals lattice with the substitution for oxygen atoms because of their high crystallinity [26,27]. Furthermore, the dose of dopant precursors would inevitably interfere in the nucleation and growth of TiO₂ single crystals [28,29]. Therefore, how to explore TiO₂ single crystals with visible-light photoactivity is big challenge for environmental pollutants treatment.

Inspired by the above-mentioned considerations, we report the first example of carbon-doped TiO₂ single crystal nanorods *via* a facile hydrothermal route. The development of the C-TiO₂ single crystal not only offers an advantage over the existed methods because they are *in situ* formed by directly carbonizing cationic polystyrene templates without additional carbon precursors, but also effectively overcomes the drawback of low solar energy utilization capacity of single crystal TiO₂. To evaluate the effectiveness of the as-prepared TiO₂ single crystal nanorods and the feasibility of applying them for water treatment, methylene blue (MB), *p*-nitrophenol (PNP), and rhodamine B (RhB), which are widely used as typical organic pollutants under visible-light irradiation [4,11,30], were selected as the target pollutants for the photocatalytic degradation tests. Excitedly, the resultant C-TiO₂ single crystal nanorods manifest a superior visible-light photocatalytic activity, far beyond the commercial P25 and carbon-doped polycrystalline TiO₂ photocatalyst.

2. Experimental

2.1. Materials

Unless otherwise noted, chemicals were obtained from J&K Chemical Company Ltd and used as received without further treatment. K₂S₂O₈, Styrene, methylene blue, Rhodamine B, *p*-nitrophenol, and absolute ethanol were bought from the Sinopharm Chemical Reagent Co., LtdS (China) and were used as received except styrene (St), which was purified with 5 wt.% NaOH solution before use. P25 (Degussa) was available from Sigma-

Aldrich Ltd. Deionised water for the reaction and analysis was collected from the Direct-Q UV System (Millipore).

2.2. The preparation of C-TiO₂ single crystal nanorods

The C-TiO₂ single crystal nanorods can be *in situ* synthesized *via* the several steps including preparation of cationic polystyrene spheres, sequential deposition of TiO₂ precursor, hydrothermal reaction, and the pyrolysis of CPS in a N₂ atmosphere at 450 °C, as shown in Scheme 1.

2.2.1. Cationic polystyrene spheres

The cationic polystyrene spheres (CPS) were prepared *via* emulsifier-free polymerization according to our previous works [31–33]: Styrene, H₂O, and K₂S₂O₈ were added into a 100 mL four-necked flask equipped with a mechanical stirrer, a Graham condenser, an N₂ inlet, and a heating mantle. After flushing the system with nitrogen gas for 20 min, the polymerization reaction was performed at 70 °C for 4 h with a stirring rate of ~400 rpm, followed by the continuous addition of cationic monomer DMC (2-(methacryloyloxy)ethyltrimethylammonium-chloride). The obtained sample was filtered and washed for three times with deionised water.

2.2.2. The synthesis of CPS/TiO₂ core/shell composites

The as-prepared CPS (4 g) was re-dispersed into absolute ethanol (40 mL) at ice-water bath, followed by the slow addition of tetrabutyl orthotitanate (TBT, 2 g) ethanol solution. After completing this, the reactive system was further kept for 24 h to allow a saturated adsorption of TBT on the surface of CPS, and then suitable ammonia (3 mL) was poured into this system to allow the sol-gel process to take place, preparing CPS/TiO₂ core/shell particles. The solid product was filtered and washed repeatedly with deionized water.

2.2.3. Hydrothermal reaction of CPS/TiO₂ core/shell composites

In a typical experiment, 240 mg CPS/TiO₂ core/shell particles was added to a Telon-lined stainless steel autoclave (50 mL) containing 8 mL of HCl (36.0–38.0%) and 10 mL of H₂O under vigorous stirring at ambient temperature. Afterwards, the sealed autoclave was heated with temperature programming from 20 °C to 180 °C at a rate of 1 °C/min and further kept for 10 h to ensure complete transformation from the core-shell composites to C-TiO₂ single crystal nanorods. The resulting precipitates were collected, washed with deionized water, dried and then calcined at 450 °C under N₂ according to the previous work [31–33].

2.3. Characterization of C-TiO₂ single crystal nanorods

The morphology and structure of C-TiO₂ single crystal nanorods were characterized using a transmission electron microscope (TEM), STEM Mapping and a scanning electron microscope (SEM), respectively. In addition, X-ray diffraction (XRD), UV-vis spectroscopy, Energy dispersive x-ray (EDX) and X-ray photoelectron spectroscopy (XPS) were used to monitor structure, morphology and components of C-TiO₂ single crystal nanorods.

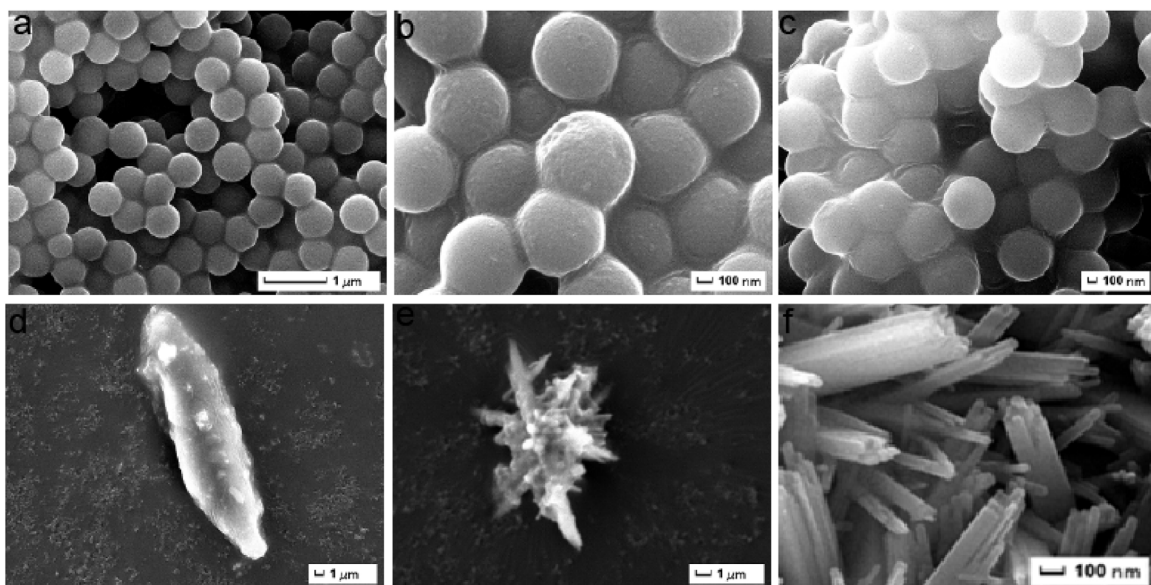


Fig. 1. The transformation process from the core-shell composites to C-TiO₂ single crystal nanorods: (a) core-shell CPS/TiO₂; (b) hydrothermal reaction (50 °C), (c) hydrothermal reaction (100 °C), (d) hydrothermal reaction (150 °C), (e) hydrothermal reaction (180 °C), and (f) calcination in N₂ (450 °C).

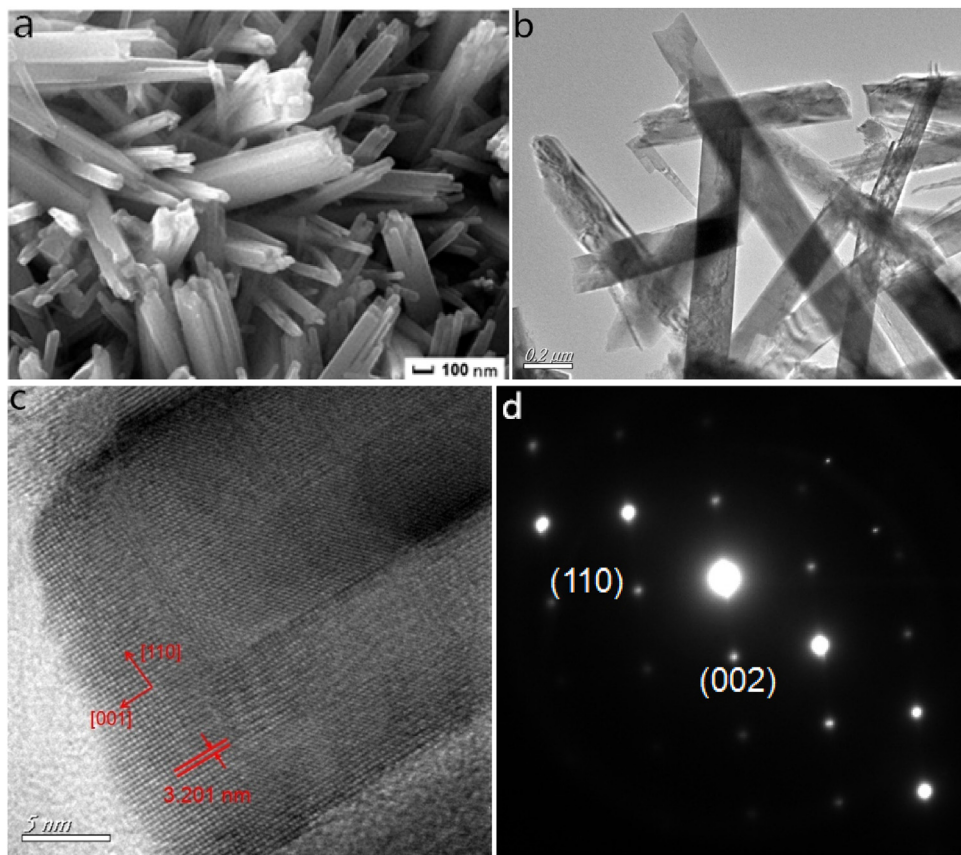


Fig. 2. SEM (a), TEM (b), high resolution TEM (c) images of C-TiO₂ single crystal nanorods and its SAED (d) pattern.

2.4. Photocatalytic activity measurement

The photocatalytic activity of TiO₂ single crystal nanorods was evaluated by the degradation of methylene blue (MB) and *p*-nitrophenol (PNP) in an aqueous solution containing 0.02 mM MB/PNP as initial concentrations and 0.2 mg/mL catalysts in 50 mL glass vessels. The visible light source used ozone-free Xe arc lamp

(XHA350W, 350 W) attached with UV cut filter ($\lambda > 420$ nm). The suspension was stirred vigorously for 30 min in the dark to establish adsorption-desorption equilibrium of MB/PNP, and then was irradiated under visible-light. Finally, samples were withdrawn periodically from the reactor, then centrifuged and analysed by recording variations in the absorption in the UV-vis spectra of MB ($\lambda = 664$ nm) [34] and PNP ($\lambda = 317$ nm) [30].

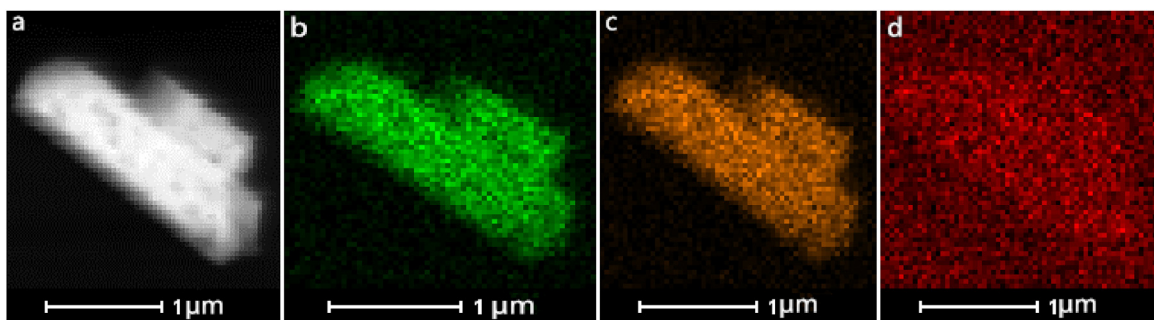


Fig. 3. STEM image (a) and EDX mapping of C-TiO₂ single crystal nanorods (b: Ti, c: O and d: C).

3. Results and discussion

3.1. The preparation of C-TiO₂ single crystal nanorods (C-TiO₂ nanorods)

To decrease the obstacle that dopants are incorporated into the TiO₂ lattice and the influence of dopant precursors on the nucleation and growth of TiO₂ single crystals [28,29], we used CPS/TiO₂ core/shell composites as the precursors of C-TiO₂ single crystal in order to improve the contact probability of TiO₂ and C precursors and possibility of the formation of C-TiO₂ single crystal, as illustrated in **Scheme 1**. Firstly, cationic polystyrene spheres (CPS) were prepared via emulsion-free polymerization by referring our previous publications [31–33]. Secondly, CPS was re-dispersed into absolute ethanol at ice-water bath, followed by the slow addition of tetrabutyl orthotitanate (TBT) ethanol solution. After completing these, suitable ammonia was added into the reaction system to allow the sol-gel process to happen, producing CPS/TiO₂ core/shell composites. Subsequently, the CPS/TiO₂ precursor was added to a Telon-lined stainless steel autoclave and heated to 180 °C for 10 h. Finally, the resultant was calcined at 450 °C in a N₂ atmosphere, *in situ* forming C-TiO₂ single crystal nanorods.

To further understand the transformation process from the CPS/TiO₂ core-shell composites to C-TiO₂ single crystal nanorods, in this paper, some samples were prepared at a certain temperature during hydrothermal reaction, and then were characterized by SEM, as shown in **Fig. 1**. After the hydrothermal reaction (50 °C) of CPS/TiO₂ composites, the CPS/TiO₂ particles begin to be fused as shown in **Fig. 1b**. With the increase in the hydrothermal temperature (100 °C), the fusion was further strengthened (**Fig. 1c**). When the hydrothermal temperature is further increased to 150 °C, the CPS/TiO₂ particles have been dissolved and fused to become a big sol, as shown in **Fig. 1d**. Excitedly, **Fig. 1e** shows that TiO₂ single crystal nanorods have been formed after the hydrothermal temperature (180 °C). The single crystal nanorods is strongly confirmed by the calcination at 450 °C, which allow one to see ordered single crystal structure as demonstrated in **Fig. 1f**.

Field-emission scanning electron microscopy (FESEM) was used to observe the morphology of the C-TiO₂ nanorods. **Fig. 2a** clearly shows that the produced TiO₂ nanorods have a cubic rod-like feature after pyrolysis of CPS under nitrogen. The TEM image indicates that its length of the as-prepared samples is about 1.5–3.6 μm (**Fig. 2b**). The selected-area electron diffraction (SAED) and high-resolution TEM (HRTEM) (sample in **Fig. 2b**) were employed to reveal the surface atomic structures. HRTEM suggests that the distance between the adjacent lattice fringes is 0.32 nm (**Fig. 2c**), which can be indexed to the interplaner distance of rutile TiO₂ (110) [35]. The corresponded SAED reveals that the C-TiO₂ nanorods are completely crystalline, displaying clearly-resolved and well-defined lattice fringes (**Fig. 2d**). EDX analysis of as-synthesized C-TiO₂ samples was performed in order to confirm the chemical composition.

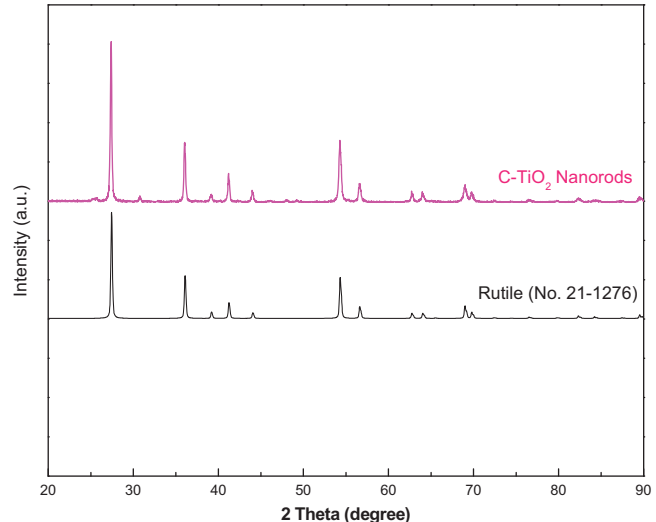


Fig. 4. XRD patterns of C-TiO₂ single crystal nanorods and the rutile of TiO₂ (No. 21-1276).

Fig. 3 indicates that the Ti and O signals are dispersed throughout the samples, whereas C signal (deep red) is mostly focused on the C-TiO₂ nanorods. All these results confirm that the TiO₂ nanorods with a single crystalline structure of rutile phase have been successfully prepared via a facile hydrothermal route.

3.2. Crystal structure and surface chemical status of C-TiO₂ single crystal nanorods

Fig. 4 demonstrates that the X-ray diffraction (XRD) patterns of standard rutile and the as-synthesized TiO₂ single crystal nanorods. According to the XRD patterns in **Fig. 4**, the well crystallized TiO₂, under N₂ calcination at 450 °C, can be classified as a tetragonal rutile structure because its reflection peaks appeared at 2θ = 27.4°(110), 36.1°(101), 41.2°(111), 44.1°(210) and 56.6°(220) are able to be assigned to the rutile of TiO₂ (No. 21-1276) [35,36], indicating C-TiO₂ rutile nanorods. In addition, the diffraction peaks of the samples are sharp and intense, indicating the highly crystalline character of the as-prepared C-TiO₂ nanorods.

X-ray photoelectron spectroscopy (XPS) measurements were used to obtain the chemical states and binding energy of elemental composition of C-TiO₂ single crystal nanorods, ascertaining thoroughly fundamental information on the interaction between the dopant (C) and TiO₂ nanorods. According to the XPS spectra in **Fig. 5a**, the three elements of O1s, Ti2p, and C1s electrons, revealing that C-TiO₂ nanorods consist of C and TiO₂. **Fig. 5b** shows that the high resolution XPS spectra of Ti2p core levels, the characteristic peak located at 458.76 eV corresponds to the Ti 2p3/2 and another

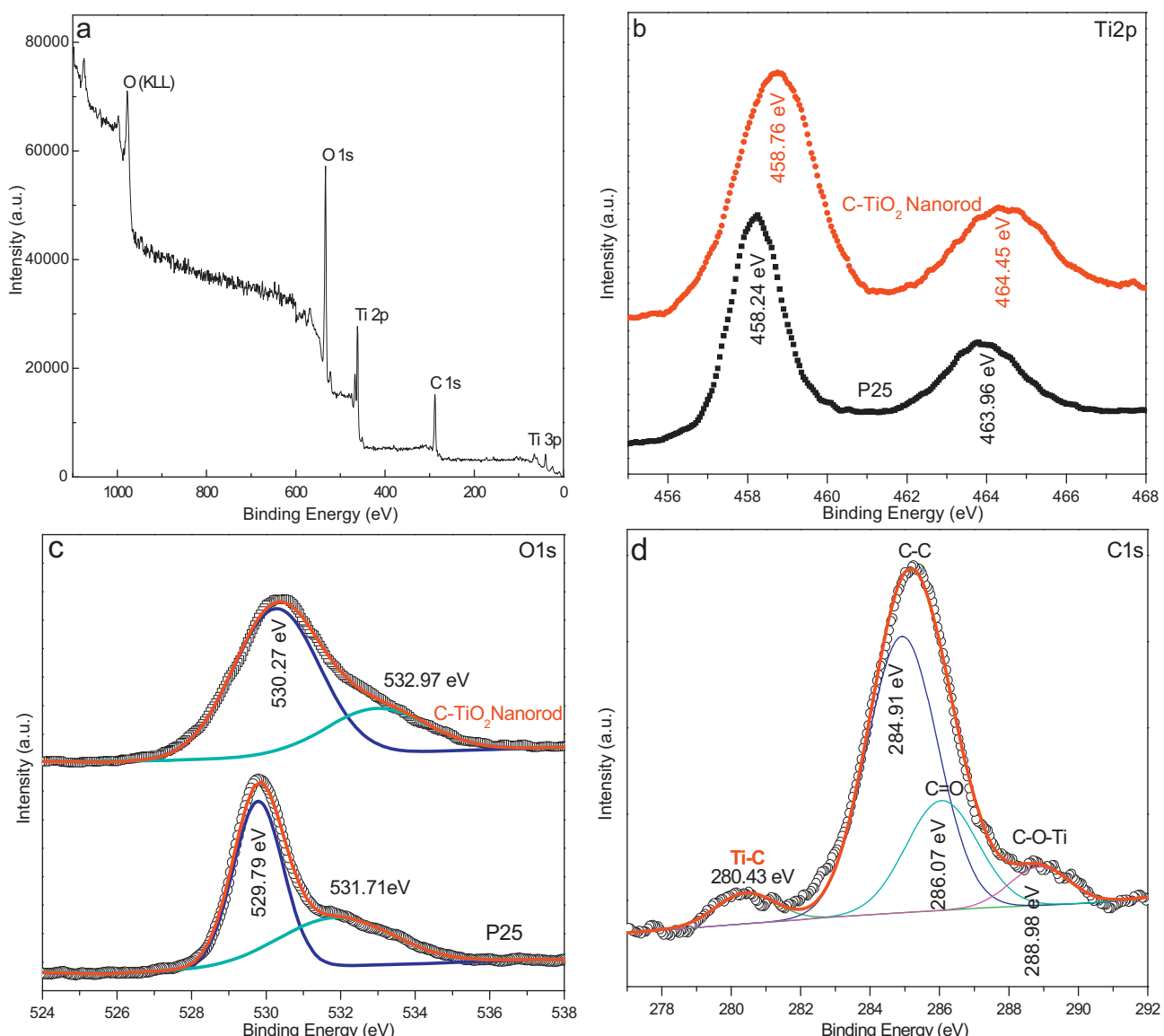


Fig. 5. (a) XPS fully scanned spectrum of the C-TiO₂ single crystal nanorods, (b) XPS spectra of Ti 2p, (c) XPS spectra of O1s, (d) XPS spectra of C1s for the C-TiO₂ nanorods.

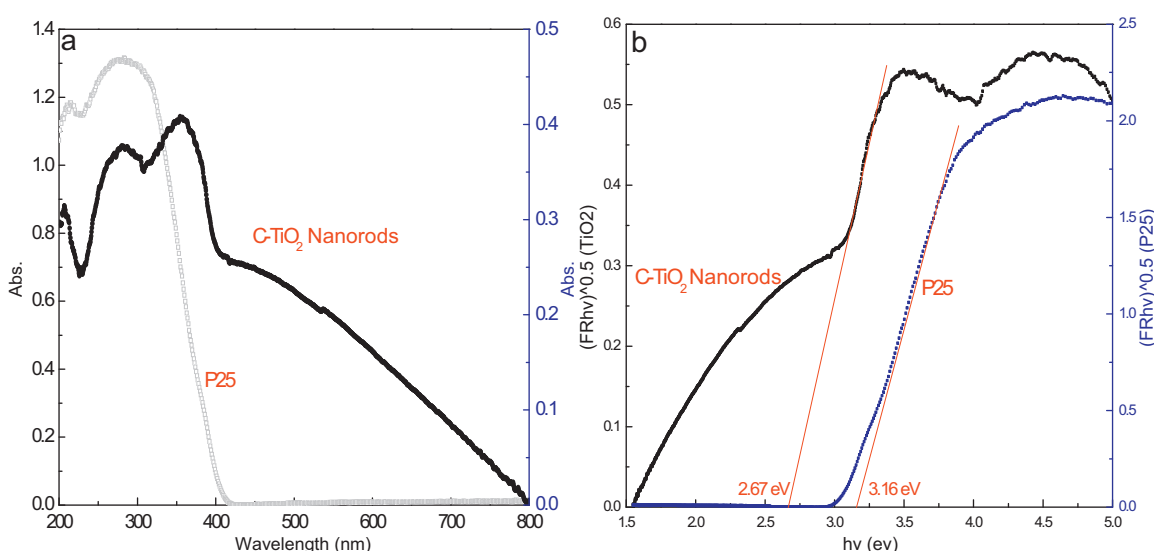


Fig. 6. (a) UV-vis absorption spectra and (b) corresponding band gap energy (E_g) of the C-TiO₂ single crystal nanorods and pure P25.

one located at 464.45 eV is indexed to Ti 2p1/2. The splitting between Ti 2p1/2 and Ti 2p3/2 is ~5.69 eV, indicating a normal state of Ti^{4+} in the C-TiO₂ single crystal nanorods [4,8]. Furthermore, a positive shift (0.49 eV) of Ti 2p1/2 binding energy can be clearly observed for C-TiO₂ nanorods as compared to the Ti 2p1/2 corresponding peak (463.96 eV) of pure P25 (Degussa) nanoparticles. The Ti 2p3/2 binding energy for the C-TiO₂ nanorods is 458.76 eV, again an increase of 0.52 eV. Understandably, the clear positive shift of binding energies is able to be ascribed to the strongly interaction between host ion Ti^{4+} and C elements, revealing lattice distortions of TiO₂ nanorods [4,37]. The high resolution O 1s spectrum (Fig. 5c) shows two peaks centered at around 530.27 eV and 532.97 eV. The former peak is indexed to bulk oxygen bound (Ti—O) in the TiO₂ single crystal lattice, while the latter peak indicates the possible surface hydroxyl groups (H—O bonds) and in carbonate species [38,39]. Similarly, the O1 s binding energies for the C-TiO₂ nanorods (Fig. 5c) exhibits a clear positive shift. This is from 529.79 eV of P25 to 530.27 eV of C-TiO₂ nanorods and from 531.71 eV in the P25 to 532.97 eV in the C-TiO₂ nanorods, which is responsible for the formation of oxygen vacancies in the TiO₂ lattice [4,40]. The XPS spectra of C1 s can be fitted to several peaks at 280.43, 284.91, 286.07, and 288.98 eV, indicating that four different chemical environments for carbon existed in the C-TiO₂ nanorods. The peak at 284.91 eV is ascribed to the residual elemental carbon formed by calcination in a N₂ atmosphere, which acts as photo-sensitizer to boost its visible light response [38,41]. Besides, the residual elemental carbon can be changed by adjusting the conditions of the pyrolysis of CPS. Therefore, the content of C in C-TiO₂ single crystal approaches to 5–16%. The two peaks at 286.07 and 288.98 eV are attributed to the existence of oxygen bound species (C=O and Ti—O—C) adsorbed on the surface of the as-prepared C-TiO₂ nanorods [38,42]. Excitedly, the peak around 280.43 eV, intrinsically resulting from the Ti—C bond, is found in the sample, strongly suggesting that the C element has been doped into the TiO₂ single crystal lattice with the substitution for oxygen atoms in our study [4].

3.3. UV-vis absorbance spectra of C-TiO₂ single crystal nanorods

Fig. 6 shows that UV-vis absorption spectra and corresponding Kubelka–Munk plots of C-TiO₂ nanorods and P25 (Degussa). As shown in Fig. 6a, un-doped P25 only absorbs UV light (200–400 nm) due to its intrinsic bandgap (~3.16 eV) [4], while as-synthesized C-TiO₂ nanorods not only have a strong absorbance in UV region (200~400 nm), but also significantly extend the visible light absorption threshold of the TiO₂ to as much as 800 nm. Clearly, the considerable enhancement of visible light absorption should be attributed to the C doping in the TiO₂ single crystal nanorods (Fig. 5d), which would introduce a series of localized occupied states into the band gap of TiO₂ lattice [40]. Band gap energy (Eg) of the as-prepared C-TiO₂ nanorods and P25 are able to be calculated by using the Kubelka–Munk method [11,40]. Fig. 6b indicates that the C-TiO₂ nanorods can effectively narrow the band gap energy of TiO₂ from 3.16 eV (P25) or ~3.0 eV (rutile TiO₂) to ~2.67 eV (C-TiO₂ nanorods), facilitating excitation of electrons from the valence band to conduction band in C-TiO₂ nanorods under visible light, resulting in a markedly enhanced photocatalytic activity.

3.4. Visible light induced photocatalytic activities

Single crystal TiO₂ can exhibit higher visible-light activity due to its continuous and ordered interior crystal structure [4,15–17]. Here, we demonstrate the potential applicability of the C-TiO₂ single crystal nanorods as an excellent photocatalyst for the degradation of methylene blue (MB), *p*-nitrophenol (PNP), and rhodamine B (RhB) under visible-light irradiation, where commercial

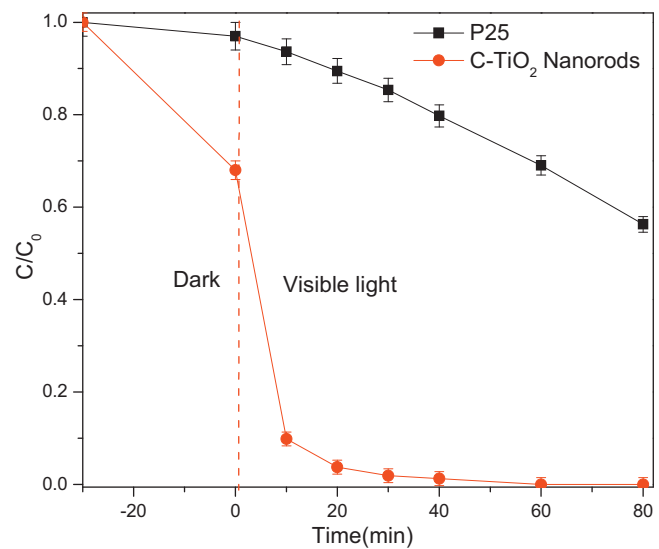


Fig. 7. Changes in the concentration of dye MB during the photocatalytic reaction in the presence of P25 and C-TiO₂ single crystal nanorods under visible light irradiation.

P25 (Degussa) is usually used as a reference photocatalyst [4,43]. Fig. 7 shows time course of the decrease in the MB dye concentration using two photocatalysts. After 10 min' visible-light radiation, the C-TiO₂ nanorods can decompose about 90.2% of MB dye, while value for the undoped P25 is very low (~6.4%). When the irradiation time is prolonged to 40 min, MB dye has been completely degraded (97.4%) by the C-TiO₂ nanorods. By contrast, Degussa P25 only degrades about 21.3% MB. Even if the irradiation time is further prolonged to 80 min, only 43.8% MB is degraded for P25, suggesting that C-TiO₂ nanorods photocatalyst has an at least twice better photocatalytic activity than P25 catalyst in decomposing MB.

For further investigation of the visible-light photocatalytic behavior, the photocatalytic activity of C-TiO₂ single crystal nanorods was also evaluated by measuring the efficiency in photocatalytic degradation of *p*-nitrophenol (PNP) in aqueous solution. As shown in Fig. 8a, with increasing illumination time, the characteristic absorption band (about 317 nm) [30] of the PNP in aqueous solution vanishes gradually in the presence of C-TiO₂ nanorods during visible-light irradiation. In contrast, there are no changes for the characteristic absorption band of PNP for Degussa P25 (Fig. 8b), suggesting that P25 is not able to decompose PNP under visible-light irradiation. Fig. 8c shows time course of the decrease in the PNP concentration using two catalysts. C-TiO₂ nanorods manifest high photocatalytic activity with 63% degradation efficiency after 80 mins. In comparison, P25 shows no photocatalytic activity under the same light irradiation, further confirming that carbon doping can improve the photocatalytic efficiency of TiO₂ in the visible-light region because carbon element can narrow the bandgap of TiO₂ nanorods (Fig. 6b) and acts as a photosensitizer [9].

To deeply evaluate the effect of crystal structure on the photocatalytic efficiency of TiO₂ nanorods, in this study, carbon-doped TiO₂ polycrystal (C-TiO₂) [4] and blue TiO_{2-x} [34] with highly efficient photoactivity were selected as reference photocatalysts. Same conditions including the dye concentration, the volume of the solution, the photocatalyst concentration, and the radiant flux were used in this experiment according to previous publications [4,34]. Table 1 suggests the comparative photocatalytic performances with C-doped TiO₂ for RhB dye degradation. Under the visible-light irradiation in a short period of 20 min, the C-doped TiO₂ samples can degrade about 56% of the original organic RhB dye. After 30 min' irradiation, RhB is degraded by 95%, completely degraded under the irradiation of visible light for 40 min [4]. By contrast, the RhB

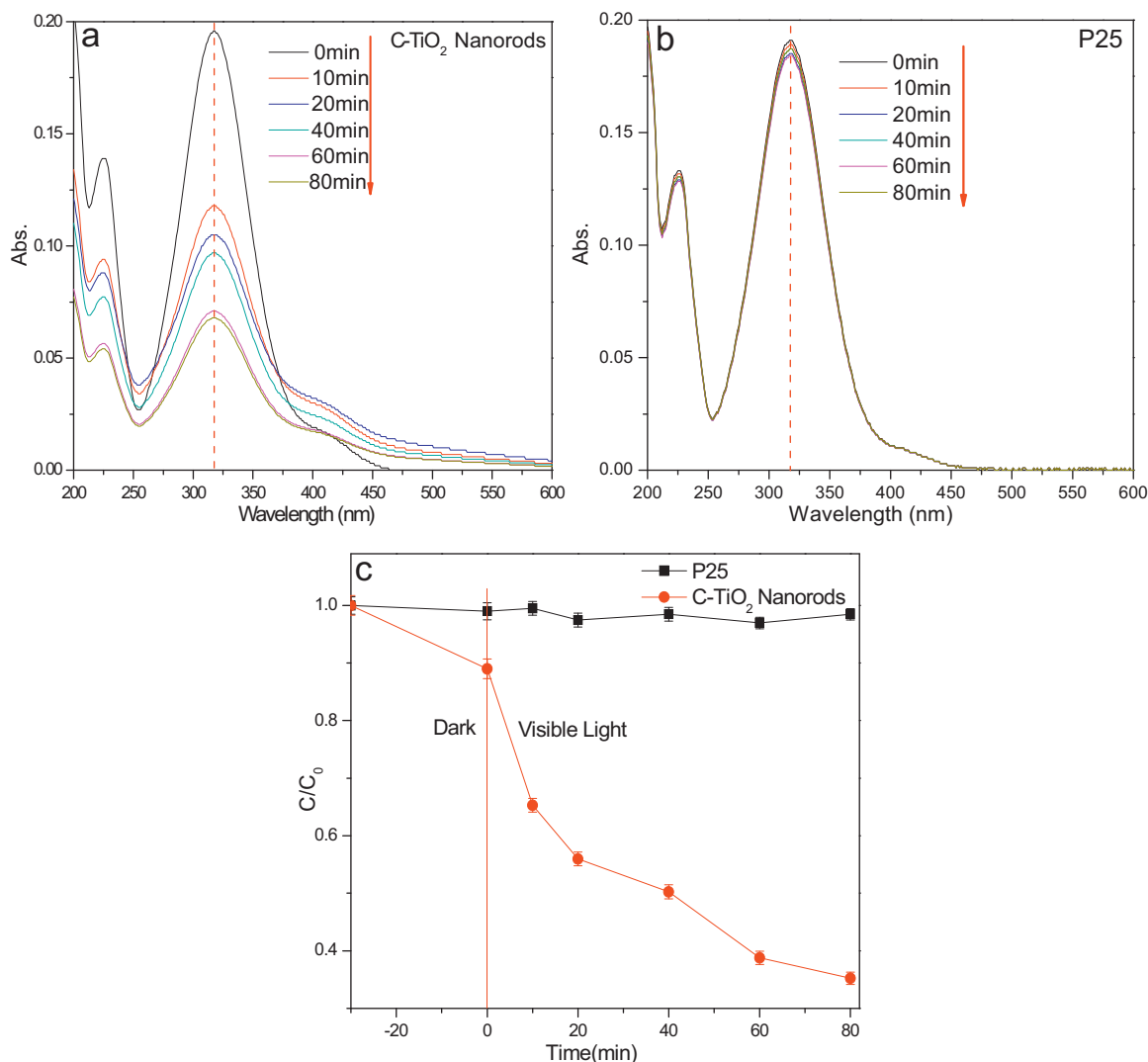


Fig. 8. UV-vis spectra of the aqueous solutions of PNP over C-TiO₂ nanorods (a), P25 (b), and (c) Changes in the concentration of PNP in the presence of C-TiO₂ nanorods and P25 under visible light irradiation.

Table 1
Comparative photocatalytic performances for RhB dye degradation under visible light irradiation.

Irradiation time (min)	P25	C-TiO ₂ [Ref. [4]]	C-TiO ₂ Nanorods
10	0.723	0.466	0.08321
20	0.569	0.055	0.00632
30	0.425	0.042	
40	0.416	0.003	
50	0.312		
60	0.098		

solution quickly lost its color in the short course of 10 min irradiation using C-TiO₂ nanorods as photocatalyst, suggesting most of the RhB is completely decomposed (91.7%). When the irradiation time is prolonged to 20 min, RhB dye has been completely

degraded (99.4%) by the C-TiO₂ nanorods. In other words, C-TiO₂ nanorods only needs 20 mins to completely degrade RhB dye, which it needs to take about 40 min in decomposing the same amount of RhB molecules for polycrystalline C-TiO₂ catalyst, suggesting that C-TiO₂ nanorods has an about twice better photocatalytic activity than carbon-doped polycrystalline TiO₂ (C-TiO₂) catalyst in decomposing RhB. Such visible-light photocatalytic efficiency is further confirmed by using bleu TiO_{2-x} as another reference photocatalyst [34], as shown in Table 2. At whole irradiation ranges, P25 used in this work exhibits a slightly lower degrad rate of the MB than the value obtained for the Degussa P25 in Ref [34], suggesting that comparative conditions have been achieved. After that, the photocatalytic efficiency of as-prepared C-TiO₂ single crystal nanorods is evaluated by degrading MB dye based on such conditions. After 60 min' irradiation, C-TiO₂ nanorods photocatalyst is

Table 2
Comparative photocatalytic performances for MB dye degradation under visible light irradiation.

Irradiation time (min)	P25	P25 [Ref. [34]]	C-TiO ₂ Nanorods	Blue TiO _{2-x} [Ref. [34]]
30	0.852	0.81	0.04782	0.33
60	0.72	0.62	0.01708	0.12
90	0.568	0.48	0.0111	0.056
120	0.42	0.38	0.0111	0.02

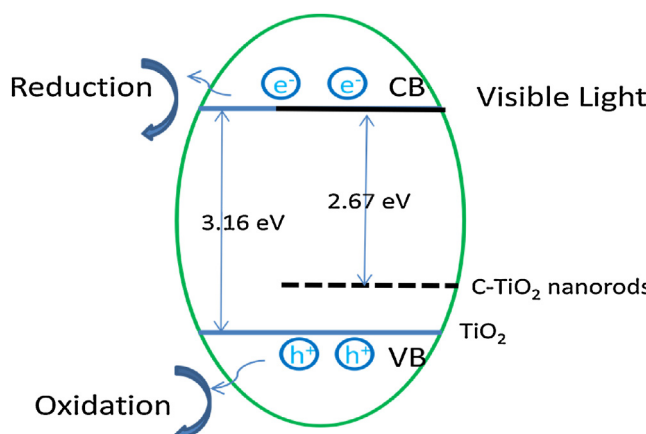


Fig. 9. The relative energy level positions of C-TiO₂ nanorods and proposed photocatalytic mechanism under visible light irradiation.

able to degrade about 98.3% of the original MB, while the blue TiO_{2-x} photocatalyst needs to take about 120 min in decomposing the same amount of MB molecules [34], suggesting that as-prepared C-TiO₂ single crystal nanorods have an about twice better photocatalytic activity than blue TiO_{2-x} catalyst in decomposing MB under same conditions.

To expound the remarkably enhanced visible-light-activity of C-TiO₂ single crystal nanorods, a possible mechanism is proposed in this work. Firstly, when the substitution for oxygen atoms by carbon atoms in the single crystal lattice of TiO₂, new impurity (carbon) is introduced between the conduction and valence band of TiO₂, and then the electrons are able to be readily promoted to the conduction band from the impurity level [44], narrowing the band gap (2.67 eV) of TiO₂, as shown in Fig. 9. When excited by visible light, photogenerated electrons more efficiently transfer to CB of TiO₂, while holes with high oxidation power are kept in the deep level of VB and degrade the dyes molecules, leading to a higher photocatalytic activity. Secondly, the residual elemental carbon adsorbed onto the surface of TiO₂ nanorods not only can improve adsorption of organic molecules, benefiting the photocatalytic performance because adsorption is normally the first step in the photocatalysis, but also can act as an efficient electron trapper to boost the electronic conductivity, lower charge transfer resistance, and induce better charge separation of the C-TiO₂ nanorods. [14,45] More importantly, single crystal structure can exhibit a much higher electronic conductivity and lower electron transfer resistance because of its continuous and ordered interior crystal structure, resulting in efficient separation and transfer of photo-generated carriers and organics decomposition [4,15–17]. Therefore, the remarkably enhanced visible-light photocatalytic activity may be ascribed to the strong synergistic effect of carbon-doping and single crystal structure in TiO₂ nanorods.

3.5. Stability of the C-TiO₂ single crystal nanorods

The stability of the photocatalyst is of importance for its practical application [14,46], and thus a series of recycling experiments, in this work, were carried out for the degradation of *p*-nitrophenol (PNP) under visible light irradiation through the observation of similar conversion efficiencies for three consecutive recycle runs by referring a previous publication [46]. As shown in Fig. 10, the result indicates that the degradation of PNP photocatalyzed by the C-TiO₂ nanorods almost remains unchanged even after three consecutive runs, suggesting that the C-TiO₂ photocatalyst exhibits a high catalytic stability for the treatment of organic contaminants in wastewater [14,46]. Clearly, the high stability/durability can be

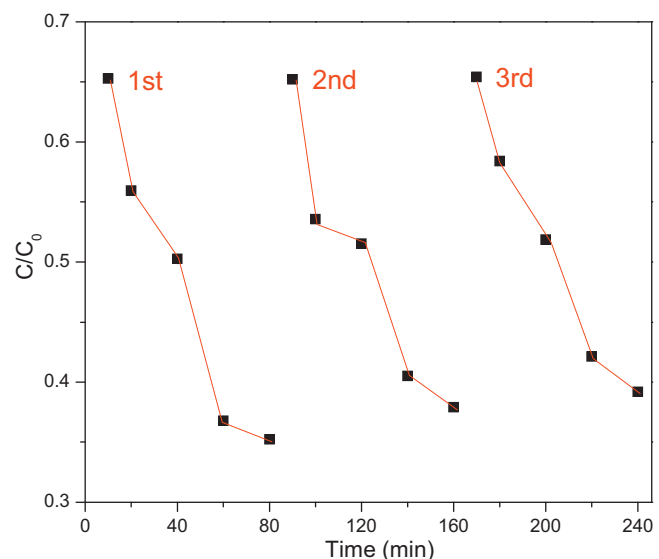


Fig. 10. Repeated runs for the decomposition of PNP using the C-TiO₂ nanorods under visible light irradiation.

attributed to the single crystal structure of C-TiO₂ nanorods, especially for rutile structure because of its unique nature including high optical stability and high chemical stability [47].

4. Conclusion

In summary, we have devised an *in situ* synthetic method to create carbon-doped TiO₂ single crystal nanorods using CPS/TiO₂ as the precursors of TiO₂ nanorods and carbon source *via* a facile hydrothermal route. Excitedly, under the pyrolysis of CPS in a N₂ atmosphere at 450 °C, carbon element is successfully doped in the place of oxygen in the TiO₂ lattice, *in situ* preparing C-TiO₂ single crystal nanorods. When used as photocatalysts for the degradation of MB, RhB and PNP under visible-light irradiation, the C-TiO₂ nanorods manifest a remarkably photocatalytic efficiency over commercial P25, C-doped TiO₂, and blue TiO_{2-x} polycrystal because of their strong synergistic effect of carbon doping and single crystal structure. Therefore, this work provides a new insight for incorporating dopants into the TiO₂ single crystal with high photocatalytic performance, considerably broadening their potential application in environmental area.

Acknowledgements

The authors would like to thank Jiangsu Natural Science Fund of China (No. BK20141299), China Postdoctoral Science Foundation (No. 2016M601744) and the innovation/entrepreneurship program of Jiangsu Province (Surencaiban [2015] 26) for financial supports to carry out this work.

References

- [1] J. Tian, Z. Zhao, A. Kumar, R. Boughton, H. Liu, Chem. Soc. Rev. 43 (2014) 6920.
- [2] J. Tian, P. Hao, N. Wei, H. Cui, H. Liu, ACS Catal. 5 (2015) 4530.
- [3] N. Wei, H. Cui, Q. Song, L. Zhang, X. Song, K. Wang, Y. Zhang, J. Li, J. Wen, J. Tian, Appl. Catal. B: Environ. 198 (2016) 83.
- [4] Y. Zhang, Z. Zhao, J. Chen, L. Cheng, J. Chang, W. Sheng, C. Hu, S. Cao, Appl. Catal. B: Environ. 165 (2015) 715–722.
- [5] W. Zhou, W. Li, J.Q. Wang, Y. Qu, Y. Yang, Y. Xie, K. Zhang, L. Wang, H. Fu, D. Zhao, J. Am. Chem. Soc. 136 (2014) 9280.
- [6] J. Chen, F. Qiu, W. Xu, S. Cao, H. Zhu, Appl. Catal. A: Gen. 495 (2015) 131.
- [7] L. Jing, W. Zhou, G. Tian, H. Fu, Chem. Soc. Rev. 42 (2013) 9509.
- [8] S. Lee, Y. Lee, D.H. Kim, J. Moon, ACS Appl. Mater. Interfaces 5 (2013) 12526.
- [9] J. Liu, Q. Zhang, J. Yang, H. Ma, M.O. Tade, S. Wang, J. Liu, Chem. Commun. 50 (2014) 13971.

[10] D.-H. Wang, L. Jia, X.-L. Wu, L.-Q. Lu, A.-W. Xu, *Nanoscale* 4 (2012) 576.

[11] Y. Shao, C. Cao, S. Chen, M. He, J. Fang, J. Chen, X. Li, D. Li, *Appl. Catal. B: Environ.* 179 (2015) 344.

[12] L. Peng, H. Zhang, Y. Bai, Y. Feng, Y. Wang, *Chem. Eur. J.* 21 (2015) 14871.

[13] J.H. Kim, D. Bhattacharjya, J. Yu, *J. Mater. Chem. A* 2 (2014) 11472.

[14] J. Zhang, M. Vasei, Y. Sang, H. Liu, J.P. Claverie, *ACS Appl. Mater. Interfaces* 8 (2016) 1903.

[15] X. Yu, H. Wang, Y. Liu, X. Zhou, B. Li, L. Xin, Y. Zhou, H. Shen, *J. Mater. Chem. A* 1 (2013) 2110.

[16] A.I. Hochbaum, P.D. Yang, *Chem. Rev.* 110 (2010) 527.

[17] C. Richter, C.A. Schmuttenmaer, *Nat. Nanotechnol.* 5 (2010) 769.

[18] C.R. Xiong, X.Y. Deng, J.B. Li, *Appl. Catal. B: Environ.* 94 (2010) 234.

[19] E.J.W. Crossland, N. Noel, V. Sivaram, T. Leijtens, J.A. AlexanderWebber, H.J. Snaith, *Nature* 495 (2013) 215.

[20] Y. Yang, G. Wang, Q. Deng, S. Kang, D.H.L. Ng, H. Zhao, *CrystEngComm* 16 (2014) 3091.

[21] N. Wu, J. Wang, D.N. Tafen, H. Wang, J. Zheng, J.P. Lewis, X. Liu, S.S. Leonard, *J. Am. Chem. Soc.* 132 (2010) 6679.

[22] Y. Liao, H. Zhang, W. Que, P. Zhong, F. Bai, Z. Zhong, Q. Wen, W. Chen, *ACS Appl. Mater. Interfaces* 5 (2013) 6463.

[23] X.H. Yang, Z. Li, C. Sun, H.G. Yang, C. Li, *Chem. Mater.* 23 (2011) 3486.

[24] X. Zheng, Q. Kuang, K. Yan, Y. Qiu, J. Qiu, S. Yang, *ACS Appl. Mater. Interfaces* 5 (2013) 11249.

[25] Z. Hong, H. Dai, Z. Huang, M. Wei, *Phys. Chem. Chem. Phys.* 16 (2014) 7441.

[26] A. Zhang, L. Long, C. Liu, W. Li, H. Yu, *Green Chem.* 16 (2014) 2745.

[27] G. Liu, H.G. Yang, X.W. Wang, L.N. Cheng, J. Pan, G.Q. Lu, H.M. Cheng, *J. Am. Chem. Soc.* 131 (2009) 12868.

[28] W.Q. Luo, C.Y. Fu, R.F. Li, Y.S. Liu, H.M. Zhu, X.Y. Chen, *Small* 7 (2011) 3046.

[29] Q.J. Xiang, J.G. Yu, W.G. Wang, M. Jaroniec, *Chem. Commun.* 47 (2011) 6906.

[30] J. Li, Q. Liu, Q. Ji, B. Lai, *Appl. Catal. B: Environm.* 200 (2017) 633.

[31] S. Cao, J. Chang, L. Fang, L. Wu, *Chem. Mater.* 28 (2016) 5596.

[32] S. Cao, J. Chen, Y. Ge, L. Fang, Y. Zhang, A.P.F. Turner, *Chem. Commun.* 50 (2014) 118.

[33] S. Cao, L. Fang, Z. Zhao, Y. Ge, S. Piletsky, A.P.F. Turner, *Adv. Funct. Mater.* 23 (2013) 2162.

[34] Q. Zhu, Y. Peng, L. Lin, C. Fan, G. Gao, R. Wang, A. Xu, *J. Mater. Chem. A* 2 (2014) 4429.

[35] H. Bai, Z. Liu, D.D. Sun, *J. Mater. Chem.* 22 (2012) 24552.

[36] H. Bai, Z. Liu, D.D. Sun, *Chem. Commun.* 46 (2010) 6542.

[37] Z. Hua, Z. Dai, X. Bai, Z. Ye, H. Gu, X. Huang, *J. Hazard. Mater.* 293 (2015) 112.

[38] Z. Jiang, W. Wei, D. Mao, C. Chen, Y. Shi, X. Lv, J. Xie, *Nanoscale* 7 (2015) 784.

[39] R. Jaiswal, J. Bharambe, N. Patel, Alpa Dashora, D.C. Kothari, A. Miotello, *Appl. Catal. B: Environ.* 168–169 (2015) 333.

[40] X. Wu, S. Yin, Q. Dong, C. Guo, H. Li, T. Kimura, T. Sato, *Appl. Catal. B: Environ.* 142–143 (2013) 450.

[41] Z. Xiong, X.S. Zhao, *J. Am. Chem. Soc.* 134 (2012) 5754.

[42] C. Cheng, X. Tan, D. Lu, L. Wang, T. Sen, J. Lei, A.M. El-Toni, J. Zhang, F. Zhang, D. Zhao, *Chem. Eur. J.* 21 (2015) 17944.

[43] W. Zhou, F. Sun, K. Pan, G. Tian, B. Jiang, Z. Ren, C. Tian, H. Fu, *Adv. Funct. Mater.* 21 (2011) 1922.

[44] M.J. Sampaio, R.R. Bacsa, A. Benyounes, R. Axet, P. Serp, C.G. Silva, A.M.T. Silva, J.L. Faria, *J. Catal.* 331 (2015) 172.

[45] H. Liu, W. Li, D. Shen, D. Zhao, G. Wang, *J. Am. Chem. Soc.* 137 (2015) 13161.

[46] Z. Jiang, C. Zhu, W. Wan, K. Qian, J. Xie, *J. Mater. Chem. A* 4 (2016) 1806.

[47] H. Bai, Z. Liu, D.D. Sun, *J. Mater. Chem.* 22 (2012) 18801.